Novel Approach to the Synthesis of Microwave Diplexers

Giuseppe Macchiarella, *Member, IEEE*, and Stefano Tamiazzo

***Abstract*—A procedure for synthesizing microwave diplexers is presented. It is based on the evaluation of the characteristic polynomials of the diplexer including the three-port junction connecting the TX and RX filters (two types of junctions are considered, suitable for waveguide and coaxial diplexers modeling). The novel method is particularly suited for small separation between the two diplexer channels: as known, this is the most difficult case in the diplexers design, due to the strong interaction between the TX and RX filters. The proposed synthesis approach offers noticeable design flexibility, as it allows the synthesis of the two composing filters independently of their connections to the diplexer, taking into account at the same time the interaction produced in the diplexer junction. Moreover the choice of the filters topology is absolutely arbitrary (the number of poles and the transmission zeros of the two filters have to be specified). The proposed method has been validated by the design and fabrication of a diplexer for global system for mobile communications base stations.**

***Index Terms*—Circuit synthesis, diplexers, microwave filters.**

I. Introduction

MICROWAVE diplexers are typically employed to connect the RX and TX filters of a transceiver to a single antenna through a suitable three-port junction. The increasing development over the last years of mobile communication systems has stimulated the need for compact high-selectivity diplexers to be used in both combiners for base stations and millimeter-wave point-to-point radio links.

Although some efforts have been made in the past for their exact synthesis [1]–[3], the most employed approach used today for the design of microwave diplexers is based on optimization. The RX and TX filters composing the diplexer are first designed independently of the diplexer (the mutual loading effects produced by the connection of the two filters to the three-port junction are so discarded). The whole diplexer structure is then numerically optimized (if possible, using full-wave modeling) by minimizing a suitably defined error function [4], [5]. Generally this approach gives satisfactory results when the initially designed diplexer presents a frequency response sufficiently close to the required mask (as in the case of well-spaced TX and RX channels).

However, when the diplexer channels are very close or even contiguous, this "brute force" approach may become too time consuming (even with the current computer-aided design (CAD) tools). The convergence could also become problematic due to the large number of "local minima," which characterizes the error function to be minimized.

To bypass such difficulties, the initial synthesis of the two filters should be carried out by taking into account the reciprocal loading, which is produced in the three-port junction [6]. Even with first-order network models for the filters and the three-port junction, such a design approach may produce acceptable results for a practical diplexer realization if tuning elements are employed in the structure [2]. In the case a high accuracy is required (e.g., when the tuning elements are not allowed), the first-order design previously described may represent a very good initial point (even for contiguous channels diplexers) for the full-wave optimization of the overall structure (in this case, the convergence to an acceptable solution can be achieved with very few iterations).

It must, however, be observed that, to the authors' knowledge, there is no synthesis procedures in the literature for diplexers employing filters with arbitrary topology (those presented in [1]–[3] refer to inline Chebyshev filters without transmission zeros).

The purpose of this study is to present a general synthesis procedure for diplexers employing TX and RX filters with arbitrary topology (i.e., producing complex transmission zeros with a predefined symmetry [8]). The interaction between the RX and TX filters through the specific three-port junction employed in the diplexer is taken into account during the synthesis and the best performances are obtained when the two channels of the diplexer are very close (and even contiguous). The procedure begin with the iterative evaluation of the polynomials associated to the overall diplexer once suitable constraints are posed on the reflection and transmission parameters of the diplexer. The characteristic polynomials [8] of the RX and TX filters are then evaluated with a polynomial fitting technique, and the synthesis of these filters is realized separately from the diplexer, using well-established methods [11], [12] (the filters topology depends on the imposed transmission zeros, assigned at the beginning of the synthesis procedure).

The derivation of the diplexer polynomials was originally introduced in [9] for a simple shunt connection of the input ports of the two filters; here, two further types of three-port junctions have been considered, well representative of practical diplexers implementations.

II. Configuration of the Diplexer

A microwave diplexer is generally composed of two bandpass filters with the two input ports connected through a three-port junction (Fig. 1).

Manuscript received September 30, 2006; revised July 7, 2006.

G. Macchiarella is with the Dipartimento di Elettronica e Informazione, Politecnico di Milano, 32-20133 Milan, Italy (e-mail: macchiar@elet.polimi.it).

S. Tamiazzo is with Andrew Telecommunication Products, 20041 Agrate Brianza, Italy (e-mail: stefano.tamiazzo@andrew.com).

Digital Object Identifier 10.1109/TMTT.2006.885909

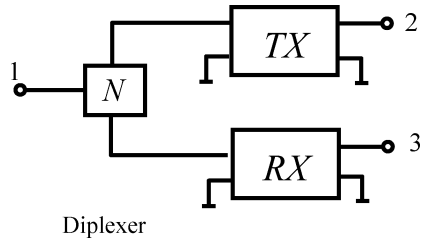

Fig. 1. General architecture of a diplexer.

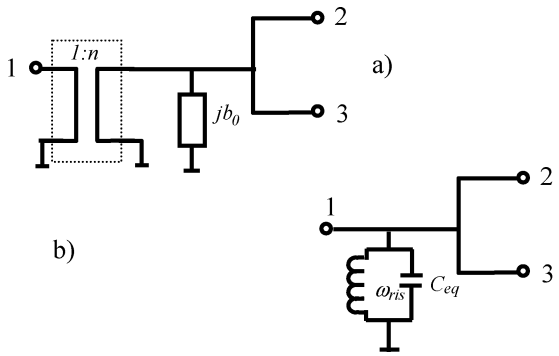

Fig. 2. Different diplexer junctions considered in this study. (a) Type-I junction. (b) Type-II junction.

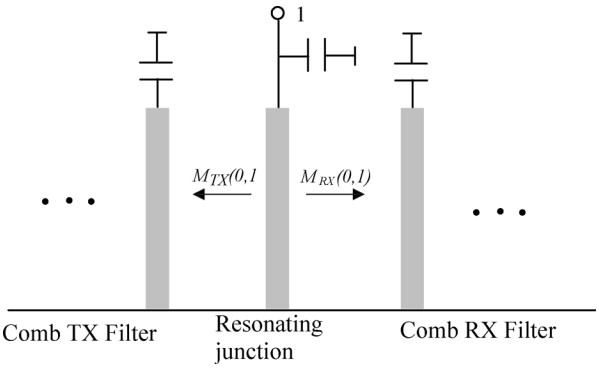

Fig. 3. Resonating junction in combline diplexers. Grey rectangles represent the metallic rods composing the coupled array. $M_{\rm TX}(0,1)$ and $M_{\rm RX}(0,1)$ are the first couplings in the two filters (not included in the junction).

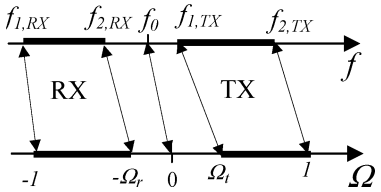

Fig. 4. Frequency mapping: $f_0 = \sqrt{f_{1,\rm RX} \cdot f_{2,\rm TX}}$, $B = f_{2,\rm TX} - f_{1,\rm RX}$. From [9].

Several structures can be employed for implementing the three-port junction, depending on the operating frequency, filter technology, electrical requirements, mechanical constraints, and so on. In this study, attention has been focused on two categories of junctions, which represent a large class of practical diplexers implementations. The equivalent circuits of these junctions are shown in Fig. 2.

The first network [see Fig. 2(a)] represents an equivalent circuit for a rectangular waveguide H-plane tee-junction (with a suitable choice of the reference sections [10]). The transformer ratio n and the susceptance b_0 can be evaluated, as a first approximation, from the waveguide dimensions with the formulas reported in [10].

The second junction type [see Fig. 2(b)] is typically found in diplexers employing coupled coaxial cavities. In this case, the common node is realized by adding an extra resonator besides those of the TX and RX filters. Fig. 3 schematically shows a possible implementation of such a junction in case of inline comb filters.

The synthesis of the diplexer is carried out in a normalized frequency domain, defined by the usual low-pass $\leftrightarrow$ bandpass frequency transformation $\Omega = (f_0/B)(f/f_0 - f_0/f)$. Fig. 4 shows the correspondence among the relevant frequency points of this transformation, together with the definition of f_0 and B. The passband limits of the RX filter are represented by $f_{1,\rm RX}$, $f_{2,\rm RX}$, while those of the TX filter are $f_{1,\rm TX}$, $f_{2,\rm TX}$. Note that the two inner passbands limits $(f_{2,\rm RX}, f_{1,\rm TX})$ are not, in general, geometrically symmetric with respect to f_0 (consequently $\Omega_r \neq \Omega_t$).

The two low-pass prototype filters (RX and TX) in the normalized frequency domain can be characterized separately from the diplexer through their characteristic polynomials. These are related to the filters' scattering parameters [8]

$$
\begin{aligned}
S_{11}^{\rm TX} &= \frac{F_{\rm TX}(s)}{E_{\rm TX}(s)} \\
S_{21}^{\rm TX} &= \frac{P_{\rm TX}(s)}{E_{\rm TX}(s)} = \frac{p_{0\rm TX} P_{\rm TX}n(s)}{E_{\rm TX}(s)} \\
S_{11}^{\rm RX} &= \frac{F_{\rm RX}(s)}{E_{\rm RX}(s)} \\
S_{21}^{\rm RX} &= \frac{P_{\rm RX}(s)}{E_{\rm RX}(s)} = \frac{p_{0\rm RX} P_{\rm RX}n(s)}{E_{\rm RX}(s)}
\end{aligned}
\tag{1}
$$

where the polynomials $F_{\rm TX}$ and $E_{\rm TX}$ have degree $np_{\rm TX}$ (order of TX filter), and the polynomials $F_{\rm RX}$ and $E_{\rm RX}$ have degree $np_{\rm RX}$ (order of TX filter). Note that these polynomials have the highest degree coefficient equal to 1 (it is assumed that the number of poles for the two filters is larger than the number of transmission zeros). The polynomials $P_{\rm TX}$ and $P_{\rm RX}$ have the highest degree coefficient given by $p_{0\rm TX}$ and $p_{0\rm RX}$, respectively (these values determine the return loss at the passband limits [8]). The TX and RX transmission zeros then completely define the normalized polynomials $P_{\rm TX}n$ and $P_{\rm RX}n$.

To evaluate the scattering parameters of the overall diplexer, the cases corresponding to the different junctions considered in this study must be analyzed separately. Note that only the scattering parameters relevant for diplexer synthesis will be considered (S_{11}, S_{21}, S_{31}).

III. Definition of Diplexer Polynomials

Assuming the overall diplexer is a lossless three-port network, four polynomials are required to define its scattering pa-

rameters in the low-pass normalized domain

$$S_{11} = \frac{n_0 N(s)}{D(s)} \quad S_{21} = \frac{p_{0t} P_t(s)}{D(s)} \quad S_{31} = \frac{p_{0r} P_r(s)}{D(s)}. \quad (2)$$

The highest degree coefficient of N, D, P_t, and P_r is imposed equal to 1 with n_0, p_{0t}, and p_{0r} suitable normalizing coefficients. Note that the roots of $D(s)$ represent the poles of the network, the roots of $N(s)$ are the reflection zeros at the common node of the diplexer (port 1 in Fig. 1), and the roots of $P_t(s)$ and $P_r(s)$ are the transmission zeros in the TX and RX path, respectively.

A. Diplexer With Type-I Junction [See Fig. 2(a)]

Let consider the input admittance at port 1

$$y_{\rm in} = n^2 \left(jb_0 + y_{\rm in}^{\rm TX} + y_{\rm in}^{\rm RX} \right) \quad (3)$$

where $y_{\rm in}^{\rm TX}$ and $y_{\rm in}^{\rm RX}$ are the admittances at the input ports of the TX and RX filters with ports 2 and 3 terminated with the reference load. These admittances can be expressed as function of the TX and RX characteristic polynomials defined in the Section II

$$\begin{aligned} y_{\rm in}^{\rm TX} &= \frac{1 - s_{11}^{\rm TX}}{1 + s_{11}^{\rm TX}} = \frac{E_{\rm TX} - F_{\rm TX}}{E_{\rm TX} + F_{\rm TX}} = \frac{D_{\rm TX}}{S_{\rm TX}} \\ y_{\rm in}^{\rm RX} &= \frac{1 - s_{11}^{\rm RX}}{1 + s_{11}^{\rm RX}} = \frac{E_{\rm RX} - F_{\rm RX}}{E_{\rm RX} + F_{\rm RX}} = \frac{D_{\rm RX}}{S_{\rm RX}} \end{aligned} \quad (4)$$

where

$$\begin{aligned} S_{\rm TX} &= \frac{(E_{\rm TX} + F_{\rm TX})}{2} \\ D_{\rm TX} &= \frac{(E_{\rm TX} - F_{\rm TX})}{2} \\ S_{\rm RX} &= \frac{(E_{\rm RX} + F_{\rm RX})}{2} \\ D_{\rm RX} &= \frac{(E_{\rm RX} - F_{\rm RX})}{2}. \end{aligned} \quad (5)$$

Let observe that $S_{\rm TX}$ and $S_{\rm RX}$ have the highest degree coefficient equal to 1 and their degree is $np_{\rm TX}$ and $np_{\rm RX}$, respectively; the degree of $D_{\rm TX}$ and $D_{\rm RX}$ is $np_{\rm TX} - 1$ and $np_{\rm RX} - 1$.

Substituting (4) in (3), the following expression for $y_{\rm in}$ is obtained:

$$y_{\rm in} = n^2 \frac{N_y}{D_y} = n^2 \frac{jb_0 S_{\rm TX} S_{\rm RX} + D_{\rm TX} S_{\rm RX} + D_{\rm RX} S_{\rm TX}}{S_{\rm TX} S_{\rm RX}}. \quad (6)$$

The parameter S_{11} of the diplexer can be expressed as function of $y_{\rm in}$ as follows:

$$S_{11} = \frac{1 - y_{\rm in}}{1 + y_{\rm in}} = \frac{D_y - n^2 N_y}{D_y + n^2 N_y}. \quad (7)$$

Substituting (6) in (7) and considering definition (2) of S_{11}, the following expressions for $N(s)$, $D(s)$, and n_0 are finally obtained:

$$\begin{aligned} N(s) &= \left[S_{\rm TX} S_{\rm RX} - n^2 \frac{D_{\rm TX} S_{\rm RX} + S_{\rm TX} D_{\rm RX}}{(1 - jn^2 b_0)} \right] \\ n_0 &= \left(\frac{1 - jn^2 b_0}{1 + jn^2 b_0} \right) \\ D(s) &= S_{\rm TX} S_{\rm RX} + n^2 \frac{D_{\rm TX} S_{\rm RX} + S_{\rm TX} D_{\rm RX}}{(1 + jn^2 b_0)}. \end{aligned} \quad (8)$$

Note that the degree of the above polynomials (the diplexer order) is equal to $np_{\rm TX} + np_{\rm RX}$. Moreover, being the highest degree coefficient of $S_{\rm TX} S_{\rm RX}$ equal to 1, the polynomials $N(s)$ and $D(s)$ are normalized as specified at the beginning of this section.

For the evaluation of the remaining polynomials, the following expressions of S_{21} and S_{31} can be derived for the considered diplexer topology:

$$\begin{aligned} S_{21} &= \frac{s_{21}^{\rm TX} \left(1 + y_{\rm in}^{\rm TX}\right)}{\frac{1}{n} + jnb_0 + n \cdot y_{\rm in}^{\rm TX} + n \cdot y_{\rm in}^{\rm RX}} \\ S_{31} &= \frac{s_{21}^{\rm RX} \left(1 + y_{\rm in}^{\rm RX}\right)}{\frac{1}{n} + jnb_0 + n \cdot y_{\rm in}^{\rm TX} + n \cdot y_{\rm in}^{\rm RX}}. \end{aligned} \quad (9)$$

Substituting (1) and (4) in the above equations and comparing with (2), P_t and P_r are derived as follows:

$$\begin{aligned} P_t(s) &= P_{{\rm TX}n} S_{\rm RX} \\ p_{0t} &= p_{0{\rm TX}} \left(\frac{n}{1 + jn^2 b_0} \right) \\ P_r(s) &= P_{{\rm RX}n} S_{\rm TX} \\ p_{0r} &= p_{0{\rm RX}} \left(\frac{n}{1 + jn^2 b_0} \right). \end{aligned} \quad (10)$$

It can be observed that the order of $P_t(s)$ (i.e., the number of transmission zeros in the TX path) is equal to $nz_{\rm TX} + np_{\rm RX}$, with $nz_{\rm TX}$ being the number of TX filter transmission zeros. This means that in addition to the zeros imposed by the TX filter, $np_{\rm RX}$ additional zeros appear in the diplexer response (the zeros of $S_{\rm RX}$). Note that these zeros do not satisfy the symmetry requirements of the imposed zeros (i.e., they are arbitrarily displaced in the complex plane). Similarly, the order of $P_r(s)$ is $nz_{\rm RX} + np_{\rm TX}$, with $nz_{\rm RX}$ being the number of RX filter transmission zeros (the same considerations on the additional zeros of P_t hold for P_r as well, exchanging $np_{\rm RX}$ with $np_{\rm TX}$ and $S_{\rm RX}$ with $S_{\rm TX}$).

B. Diplexer With Type-II Junction [See Fig. 2(b)]

To simplify the low-pass equivalent circuit for the type-II junction, it is assumed that the resonating frequency f_{ris} of the junction node coincides with f_0. The shunt resonator is then replaced in the normalized frequency domain by the capacitance c_0. The diplexer polynomials can be derived analytically as in the previous case, obtaining the following expressions:

$$\begin{aligned} N(s) &= sS_{\rm TX} S_{\rm RX} - \frac{1}{c_0}(S_{\rm TX} S_{\rm RX} - D_{\rm TX} S_{\rm RX} - S_{\rm TX} D_{\rm RX}) \\ n_0 &= -1 \\ D(s) &= sS_{\rm TX} S_{\rm RX} + \frac{1}{c_0}(S_{\rm TX} S_{\rm RX} + D_{\rm TX} S_{\rm RX} + S_{\rm TX} D_{\rm RX}) \\ P_t(s) &= P_{{\rm TX}n} S_{\rm RX} \\ p_{0t} &= \frac{p_{0{\rm TX}}}{c_0} \\ P_r(s) &= P_{{\rm RX}n} S_{\rm TX} \\ p_{0r} &= \frac{p_{0{\rm RX}}}{c_0}. \end{aligned} \quad (11)$$

Let observe that, in this case, the number of poles (and reflection zeros) is $np_{\rm TX}+np_{\rm RX}+1$ because of the capacitance c_0. The number of transmission zeros at infinity in the TX and RX path of the diplexer is also increased by one, again due to the resonant nature of the junction node. Finally, the considerations regarding the number of P_t and P_r roots presented for the type-I junction hold for type II as well.

IV. Procedure for Evaluating the Characteristic Polynomials

In Section III, analytical expressions have been derived, which relate the overall diplexer polynomials to the characteristic polynomials of the RX and TX filters defined in (2). A procedure will be now introduced, allowing the evaluation of these latter polynomials, once suitable constraints are posed on the reflections and transmission parameters of the diplexer. In this way, the reciprocal loading produced by each filter on the other through the three-port junction is taken into account during the synthesis of the filters (which can be carried out independently of the diplexer, employing one of the well-established methods available in the literature [8], [11], [12]).

Let consider the first constraint, which is imposed on the reflection coefficient at the input port of the diplexer: the typical requirement is constituted by an equiripple response in the RX and TX channels with a prescribed minimum level of return loss. Unfortunately, to the authors' knowledge, an analytical method does not exist for the evaluation of the reflection zeros at the input port of the diplexer (i.e., the roots of $N(s)$), producing a perfect equiripple response in the TX and RX bands. An approximate solution has been found, however, by assigning to these zeros the pure imaginary values resulting from the synthesis of the TX and RX filters, generated independently of presence of the diplexer, with a general Chebyshev characteristic (including, if desired, complex transmission zeros). Surprisingly by using this approach, at the end of the synthesis procedure, a deviation of no more than 2 dB between the return loss actually presented by the synthesized diplexer and the ideal equiripple response has been obtained.

In case of a type-II junction, one of the reflection zeros is imposed by the capacitance c_0. This zero has to be specified in the normalized domain (s_{co}), with the requirement that it does not affect the quasi-equiripple response determined by the other (pure imaginary) reflection zeros. This goal is achieved by assigning to s_{co} a pure real value (a good choice has proven to be $s_{co}=1.5$). This condition determines the value of c_0.

The other constraint concerns the transmission zeros of the TX and RX filters: it is assumed that these zeros (i.e., the roots of polynomials $P_{{\rm TX}n}(s)$ and $P_{{\rm RX}n}(s)$) are imposed *a priori*. As a consequence, these zeros also appear in S_{21}- and S_{31}-parameters of the diplexer [from (10) or (11)].

A. Evaluation of the Diplexer Polynomials

The synthesis procedure consists first in the derivation of the diplexer polynomials $N(s)$, $D(s)$, $P_t(s)$, and $P_r(s)$ having initially assigned the junction topology, the reflection zeros at the input port of the diplexer, and the transmission zeros of the TX and RX filters. Note that, assuming a lossless overall diplexer, the unitary condition of the scattering matrix imposes that

$$D(s)\cdot D^*(-s)=|n_0|^2N(s)\cdot N^*(-s)+|p_{0r}|^2P_r(s)\cdot P_r^*(-s)+|p_{0t}|^2P_t(s)\cdot P_t^*(-s). \quad (12)$$

Note also that $N(s)\cdot N^*(-s)$ depends only on the imposed reflection zeros being $|n_0|=1$ for both junction types.

The evaluation of the diplexer polynomials is carried out iteratively according to the following steps.

Step 1) Initialization: the RX and TX filters are synthesized independently of the diplexer with a general Chebyshev characteristic (i.e., the polynomials $F_{\rm TX}^0$, $E_{\rm TX}^0$, $P_{\rm TX}^0$, $F_{\rm RX}^0$, $E_{\rm RX}^0$, and $P_{\rm RX}^0$ are generated given the number of poles $(np_{\rm TX}, np_{\rm RX})$, the return loss in the two channels, and the transmission zeros of the two filters). To this purpose, well-established techniques are available in the literature [8], [11], [12]. The diplexer reflection zeros are obtained from the roots of $F_{\rm TX}^0$ and $F_{\rm RX}^0$ (for a type-II junction, a further zero $s_{co}=1.5$ is added). An initial estimate of $S_{\rm TX}$ and $S_{\rm RX}$ is then available from the above polynomials.

Step 2) Begin iteration: P_t and P_r are evaluated using polynomial convolution: $P_t=\mathrm{conv}(P_{{\rm TX}n},S_{\rm RX})$ and $P_r=\mathrm{conv}(P_{{\rm RX}n},S_{\rm TX})$

Step 3) Evaluation of $|p_{0r}|$ and $|p_{0t}|$: the required return loss in the two channels ($\mathrm{RL}_{\rm TX}$ and $\mathrm{RL}_{\rm RX}$) is imposed at the normalized frequencies $s=\pm j$

$$\frac{|N(j)|^2}{|N(j)|^2+|p_{0r}|^2\cdot|P_r(j)|^2+|p_{0t}|^2\cdot|P_t(j)|^2}=10^{-\mathrm{RL}_{\rm TX}/10}$$
$$\frac{|N(-j)|^2}{|N(-j)|^2+|p_{0r}|^2\cdot|P_r(-j)|^2+|p_{0t}|^2\cdot|P_t(-j)|^2}=10^{-\mathrm{RL}_{\rm RX}/10}. \quad (13)$$

$|p_{0r}|^2$ and $|p_{0t}|^2$ are obtained by solving the above linear system. Applying the spectral factorization technique to (12), $D(s)$ is then evaluated from its roots (the poles of the diplexer).

Step 4) New estimation of $S_{\rm TX}$ and $S_{\rm RX}$: the roots of the polynomial $(aN(s)+bD(s))/2\doteq S_{\rm TX}(s)\cdot S_{\rm RX}(s)$ are computed with $a=1-jn^2\cdot b_0$ and $b=1+jn^2\cdot b_0$ (type-I junction) or $b=-a=1$ (type-II junction). The roots are sorted with increasing imaginary part. The first $np_{\rm RX}$ roots are assigned to $S_{\rm RX}$ and the last $np_{\rm TX}$ roots are assigned to $S_{\rm TX}$ (it is assumed that the RX band is below the TX band). $S_{\rm TX}$ and $S_{\rm RX}$ are generated from their roots (the highest degree coefficients are equal to 1 for both of these polynomials).

Step 5) Convergence verification: the roots of $S_{\rm TX}$ and $S_{\rm RX}$ are compared with those evaluated at the previous iteration. The procedure iterates from point 2 until

the maximum relative difference between new and old roots is below a prescribed level.

It has been found that the convergence is typically obtained within 5–10 iterations.

In case of a type-II junction, parameter c_0 is not given explicitly (the reflection zero s_{co} is instead specified). However, the value of c_0 can be derived from inspection of $N(s)$ and $D(s)$ (11)

$$D_{(2)} = -N_{(2)} = \frac{1}{c_0} \tag{14}$$

where $N_{(2)}$ and $D_{(2)}$ represent the second highest degree coefficient of the two polynomials.

B. Computation of R_X and T_X Filter Polynomials

The second step in the diplexer synthesis is the computation of the polynomials characterizing the TX and RX filters (i.e., $P_{\rm TX}$, $F_{\rm TX}$, $E_{\rm TX}$, $P_{\rm RX}$, $F_{\rm RX}$, and $E_{\rm RX}$). $P_{\rm TX}$ and $P_{\rm RX}$ can be immediately computed at the end of the iterative procedure. In fact, $P_{{\rm TX}n}$ and $P_{{\rm RX}n}$ are known from the imposed transmission zeros, and the coefficients $p_{0{\rm TX}}$ and $p_{0{\rm RX}}$ can be evaluated from p_{0t} and p_{0r} using (10) or (11) as follows:

$$\begin{aligned} p_{0{\rm TX}} &= p_{0t}\left(\frac{1+jn^2b_0}{n}\right) \\ p_{0{\rm RX}} &= p_{0r}\left(\frac{1+jn^2b_0}{n}\right) \quad \text{Type-I junction} \\ p_{0{\rm TX}} &= c_0 \cdot p_{0t} \\ p_{0{\rm RX}} &= c_0 \cdot p_{0r} \quad \text{Type-II junction.} \end{aligned} \tag{15}$$

To obtain the remaining polynomials, it is necessary to first evaluate the polynomials $D_{\rm RX}$ and $D_{\rm TX}$, as described in the following.

Let $zS_{\rm TX}$ and $zS_{\rm RX}$ be the roots of $S_{\rm TX}$ and $S_{\rm RX}$, respectively (note that $S_{\rm TX}$ and $S_{\rm RX}$ are known at the end of the iterative procedure). Using (8) or (11), the values $D_{\rm TX}(zS_{\rm TX})$ and $D_{\rm RX}(zS_{\rm RX})$ can be computed from the following expressions:

$$\begin{aligned} D(zS_{\rm TX}) &= A \cdot D_{\rm TX}(zS_{\rm TX})S_{\rm RX}(zS_{\rm TX}) \Rightarrow D_{\rm TX}(zS_{\rm TX}) \\ &= \frac{D(zS_{\rm TX})}{A \cdot S_{\rm RX}(zS_{\rm TX})} \\ D(zS_{\rm RX}) &= A \cdot D_{\rm RX}(zS_{\rm RX})S_{\rm TX}(zS_{\rm RX}) \Rightarrow D_{\rm RX}(zS_{\rm RX}) \\ &= \frac{D(zS_{\rm RX})}{A \cdot S_{\rm TX}(zS_{\rm RX})} \end{aligned} \tag{16}$$

where A is given by $n^2/(1+jn^2b_0)$ for a type-I junction and by $1/c_0$ for a type-II junction. Now, from the knowledge of the degree of $D_{\rm RX}$ and $D_{\rm TX}$ ($np_{\rm RX}-1$ and $np_{\rm TX}-1$, respectively), one finds that the number of unknowns (the coefficients of these polynomials) is just equal to the computed values with (16). A least square polynomial interpolation then allow the derivation of $D_{\rm TX}$ and $D_{\rm RX}$ as follows:

$$\begin{aligned} D_{\rm TX}(s) &= \text{polyfit}\,(zS_{\rm TX}, D_{\rm TX}(zS_{\rm TX}), np_{\rm TX}-1) \\ D_{\rm RX}(s) &= \text{polyfit}\,(zS_{\rm RX}, D_{\rm RX}(zS_{\rm RX}), np_{\rm RX}-1)\,. \end{aligned} \tag{17}$$

Finally, $F_{\rm TX}$, $E_{\rm TX}$, $F_{\rm RX}$, and $E_{\rm RX}$ are obtained from the sum and the difference of $S_{\rm TX}$, $D_{\rm TX}$ and $S_{\rm RX}$, $D_{\rm RX}$ as follows:

$$\begin{aligned} F_{\rm TX}(s) &= S_{\rm TX}(s) - D_{\rm TX}(s) \\ E_{\rm TX}(s) &= S_{\rm TX}(s) + D_{\rm TX}(s) \\ F_{\rm RX}(s) &= S_{\rm RX}(s) - D_{\rm RX}(s) \\ E_{\rm RX}(s) &= S_{\rm RX}(s) + D_{\rm RX}(s). \end{aligned} \tag{18}$$

C. Consideration on the Accuracy

As in all design approaches of microwave filters based on the equivalence between lumped and distributed models, the accuracy of the proposed synthesis method depends, first of all, on the normalized bandwidth employed in the low-pass–bandpass transformation. In this case, such bandwidth depends on the difference between the outer bandpass frequencies of the TX and RX filters: as a consequence, the accuracy increases by reducing both the TX and RX bandwidth and their separation. The best performance of the proposed synthesis approach is then expected with contiguous channel diplexers composed of narrowband filters.

V. Design of Diplexers With Type-I Junction

Here, the circuit design of a waveguide diplexer with an H-plane tee-junction will be employed to demonstrate the effectiveness of the novel synthesis technique. The RX and TX filters are all poles, inline Chebyshev filters composed of waveguide cavities coupled through inductive iris [13]. Their design will be carried out with reference to the classical network model constituted by waveguide sections cascaded with shunt-inductive reactances [13].

The design specifications for the waveguide diplexer are the following (two almost contiguous bands have been required, being the new synthesis technique specifically suited for this condition).

- RX filter (all poles):
  Passband 14.9–15.1 GHz; return loss $({\rm RL}_{\rm RX})$: 20 dB.
  Number of poles $(np_{\rm TX})$: 7.
- TX filter (all poles):
  Passband 15.15–15.35 GHz; return loss $({\rm RL}_{\rm RX})$: 20 dB.
  number of poles $(np_{\rm TX})$: 7.

The waveguide WR62 has been selected ($a = 15.8$ mm, $b = 7.9$ mm), determining the following values for the parameters of the tee-junction equivalent circuit [10] $n = 1.47$ and $b_0 = -0.171$.

The characteristic polynomials of the diplexer have been evaluated with the iterative procedure illustrated in Section IV, ob-

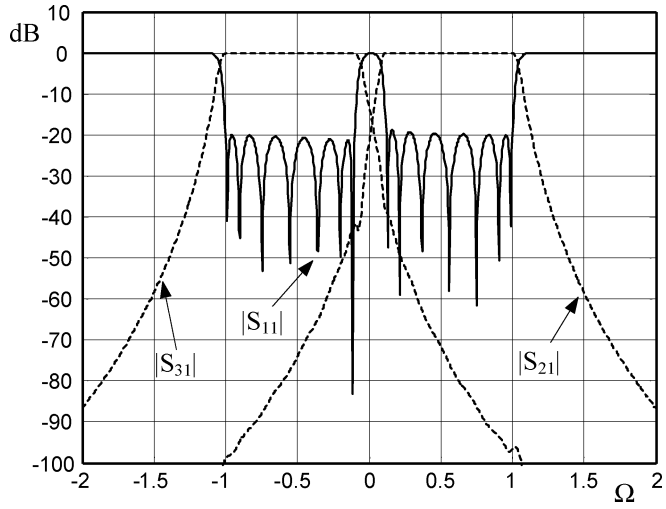

Fig. 5. Computed response of the waveguide diplexer (polynomial model).

taining the following values (the polynomial coefficients are reported in descending order):

$$
\begin{aligned}
n_0.N =& [0.76+0.65i,\ 0.033-0.039i,\ 2.166+1.854i,\\
& 0.09-0.105i,\ 2.31+1.976i,\ 0.0886-0.103i,\\
& 1.14+0.977i,\ 0.0391-0.04561i,\ 0.265+0.226i,\\
& 0.0076-0.0089i,\ 0.026+0.022i,\\
& 5.5e-4-6.48e4i,\ 9.29e-4+7.95e-4i,\\
& 1.055e-5-1.23e-5i,\ 8.87e-6+7.59e-6i]\\
D =& [1, 1.77-0.051i,\ 4.417-0.104i,\ 5.3-0.242i,\\
& 6.724-0.3119i,\ 5.61-0.376i,\ 4.425-0.326i,\\
& 2.51-0.24i,\ 1.25-0.14i,\ 0.44-0.065i,\\
& 0.128-0.02248i,\ 0.024-5.7e-3i,\\
& 3.27e-3-9.5e-4i,\ 2.26e-4-9.21e-5i,\\
& 1.123e-5-4.25e-6i]\\
P_t =& [1\ 0.455+3.9i, -6.027+1.53i, -1.97-4.6i,\\
& 1.833-1.21i,\ 0.359+0.351i,\ -0.0275+0.046i,\\
& -0.0018-0.000579i]\\
p_{0t} =& 4.717e-4+1.743e-4i,\\
P_r =& [1\ 0.43-4.29i,\ -7.337-1.6i,\ -2.31+6.37i,\\
& 2.95+1.6i,\ 0.565-0.7i,\ -0.076-0.091i,\\
& -0.005+0.0027i]\\
p_{0r} =& 4.336e-4+1.6e-4i.
\end{aligned}
$$

Fig. 5 shows the computed polynomial response of the diplexer, obtained from the scattering parameters (2). Note that the maximum deviation of the return loss from the ideal equiripple condition is less than 2 dB.

The following step in the diplexer design has been the synthesis of the low-pass prototype of the RX and TX filters from the computed characteristic polynomials $P_{\rm TX}$, $F_{\rm TX}$, and $E_{\rm TX}$ and $P_{\rm TX}$, $F_{\rm RX}$, and $E_{\rm RX}$ (note that $P_{\rm TX}$ and $P_{\rm RX}$ coincide with the coefficients $p_{0\rm TX}$ and $p_{0\rm RX}$ because are all pole filters are considered here). Using well-known techniques available in the literature [8], the normalized coupling matrix M of the inline canonical prototype is first derived from the filter polynomials

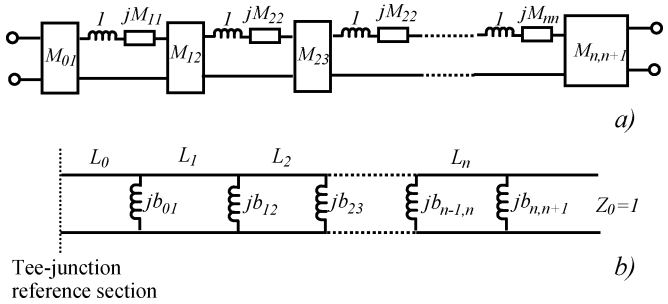

Fig. 6. Equivalent circuits for waveguide filters. (a) Prototype topology defined by the coupling matrix elements. The $M_{i,i+1}$ blocks are impedance inverters; the $M_{i,i}$ elements are frequency invariant reactances. (b) Denormalized waveguide filter topology [13], [14].

(Fig. 6(a) shows the correspondence between the prototype elements and the coupling matrix elements $M_{i,j}$).

The parameters of the waveguide filter model [see Fig. 6(b)] are then obtained de-normalizing the prototype with the following formulas [13], [14]:

$$
\begin{aligned}
f_{0,k} &= f_0\left[\sqrt{1-\left(\frac{B_n M_{k,k}}{2}\right)^2}-\frac{B_n M_{k,k}}{2}\right]\\
F_k &= \sqrt{1-(f_c/f_{0,k})^2}, \qquad k=1,\ldots,n\\
K_{0,1} &= \frac{M_{0,1}}{F_1}\sqrt{B_n\frac{\pi}{2}}\\
K_{n,n+1} &= \frac{M_{n,n+1}}{F_n}\sqrt{B_n\frac{\pi}{2}}\\
K_{k,k+1} &= B_n\frac{\pi}{2}\frac{M_{k,k+1}}{F_k F_{k+1}}, \qquad k=1,\ldots,n-1\\
b_{k,k+1} &= -\left(\frac{1}{K_{k,k+1}}+K_{k,k+1}\right)\\
\varphi_{k,k+1} &= -\tan^{-1}\left(\left|\frac{2}{b_{k,k+1}}\right|\right)\\
\Delta L_{k,k+1} &= \frac{\varphi_{k,k+1}}{2\pi}\frac{c/f_0}{\sqrt{1-(f_c/f_0)^2}}, \qquad k=0,\ldots,n\\
L_k &= \frac{c/f_0}{2F_k}+\frac{(\Delta L_{k-1,k}+\Delta L_{k,k+1})}{2}, \qquad k=1,\ldots,n.
\end{aligned}
\tag{19}
$$

where $B_n = B/f_0$ (B and f_0 are defined in Fig. 4), c is the velocity of light, and f_c is the cutoff frequency of $\rm TE_{10}$: $f_c = c/(2a)$. Let us observe that the TX and RX filters synthesized here are not synchronous (i.e., the cavities resonate at frequencies $f_{0,k}$ are different from each other). We also observe that, in order to obtain the required impedance levels at the reference sections of the tee-junction, a further unit inverter (realized with a waveguide section of length $\lambda_{g0}/4$) has been introduced at the filters inputs. The length L_0 of the waveguide section in Fig. 5(b) is then given by

$$
L_0 = \frac{c/f_0}{4\sqrt{1-(f_c/f_0)^2}}\left(1+\frac{\varphi_{0,1}}{\pi}\right). \tag{20}
$$

Table I reports the matrices $M_{\rm TX}$ and $M_{\rm RX}$ computed for the two filters (the elements of the first two diagonals are reported

TABLE I
COUPLING MATRIX ELEMENTS OF SYNTHETIZED TX AND RX FILTERS

k	$M_{TX}(k,k)$	$M_{TX}(k\text{-}1,k)$	$M_{RX}(k,k)$	$M_{RX}(k\text{-}1,k)$
1	-0.8827	0.5381	0.6066	0.4195
2	-0.5888	0.3484	0.5609	0.3390
3	-0.5678	0.2575	0.5500	0.2665
4	-0.5631	0.2458	0.5495	0.2534
5	-0.5619	0.2468	0.5495	0.2538
6	-0.5621	0.2622	0.5490	0.2702
7	-0.5638	0.3622	0.5464	0.3773
8	-	0.6556	-	0.6748

TABLE II
PARAMETERS OF THE DENORMALIZED TX AND RX FILTERS

k	*TX Filter*		*RX Filter*	
	L_k *(mm)*	$b_{k,k+1}$	L_k *(mm)*	$b_{k,k+1}$
0	5.77	-6.6	5.90	-8.41
1	11.77	-37.7	12.35	-37.78
2	12.37	-50.89	12.73	-48.10
3	12.41	-53.29	12.75	-50.59
4	12.41	-53.08	12.76	-50.51
5	12.41	-49.95	12.75	-47.44
6	12.37	-36.15	12.71	-33.97
7	11.73	-5.34	12.04	-5.12

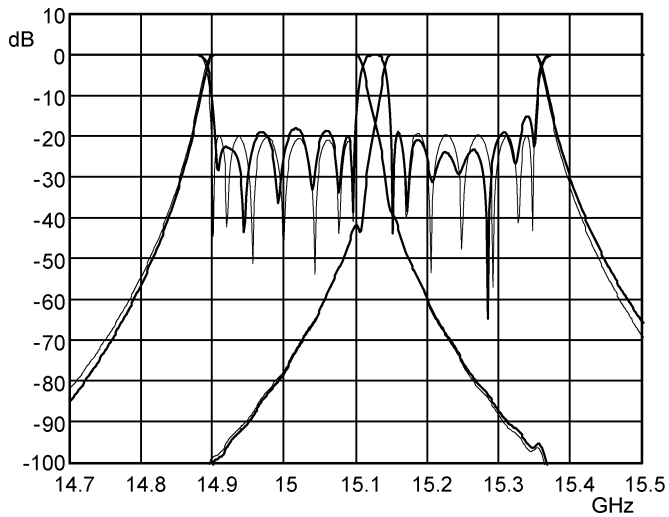

Fig. 7. Simulated response of the designed waveguide diplexer (bold curve). TX and RX filters are represented by the circuit model in Fig. 6(b). For comparison, the ideal polynomial response is also reported (light curve).

because all the others elements are equal to zero); the parameters L_k and $b_{k,k+1}$ are given in Table II.

The result of the diplexer simulation, based on circuit models, is shown in Fig. 7: the agreement with the ideal polynomial response (also reported in Fig. 7) can be considered satisfactory (the discrepancies are mainly due to the variation with frequency of the equivalent inverters parameter [14]). It has then been assessed that the novel design procedure produces satisfying results when the waveguide diplexer is represented with a network elementary model. Nevertheless the obtainable accuracy is typically acceptable for a practical diplexer realization if tuning elements (screws) are included in the fabricated device [2]. When an high accuracy is instead required (no tuning elements allowed), the design results obtained here represent a very good starting point for optimization procedures based on full-wave

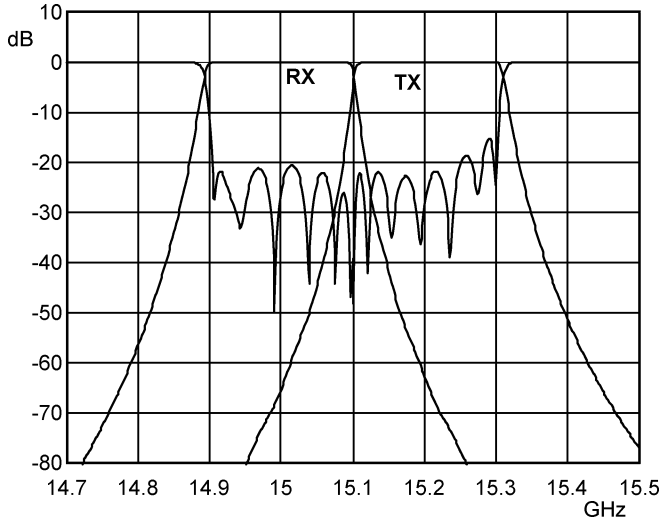

Fig. 8. Simulated response of the contiguous waveguide diplexer designed with the novel procedure.

characterization of the overall diplexer structure [4], [5], [7]. As previously stated, in case of contiguous-band diplexers, a good starting point for such optimization procedures is a mandatory requirement for obtaining the convergence to an acceptable solution. To give an idea of the starting point obtainable with the novel design procedure, the waveguide diplexer considered here has been redesigned imposing two contiguous bandwidths: the corresponding simulated response is shown in Fig. 8.

VI. DESIGN OF DIPLEXRS WITH TYPE-II JUNCTION

Here, the design of a diplexer with a type-II junction is illustrated. The technology concerned here is that of the generalized comb filters employed in base stations for mobile communication [17]. As depicted in Fig. 3, the resonating node is realized by means of an additional resonator coupled to the first RX and TX cavities.

The following requirements considered for the diplexer synthesis refer to a typical global system for mobile communications (GSM) combiner operating at 1900 MHz.

- RX filter:
  Number of poles: 10.
  Band: 1845.5–1915.5 MHz.
  Return loss $(\mathrm{RL}_{\mathrm{RX}})$: 22 dB.
  Transmission zeros (MHz): 1830, 1928.5, 1932.1, 1942.8.
- TX filter:
  Number of poles: 9.
  Band: 1925–1992 MHz.
  Return loss $(\mathrm{RL}_{\mathrm{TX}})$: 22 dB.
  Transmission zeros (MHz): 1890, 1905, 1910.

Note that the high selectivity required calls for several transmission zeros (both in TX and RX filters). These zeros are implemented though couplings between nonadjacent resonators.

The design procedure begins, as in the previous case, with the evaluation of the diplexer polynomials $N(s)$, $D(s)$, $P_r(s)$, and $P_t(s)$. The imposed zeros of $N(s)$ (reflection zeros of the diplexer) have been obtained from the roots of the characteristic polynomials F^0_{TX} and F^0_{RX}. These polynomials (with P^0_{TX}, E^0_{TX}

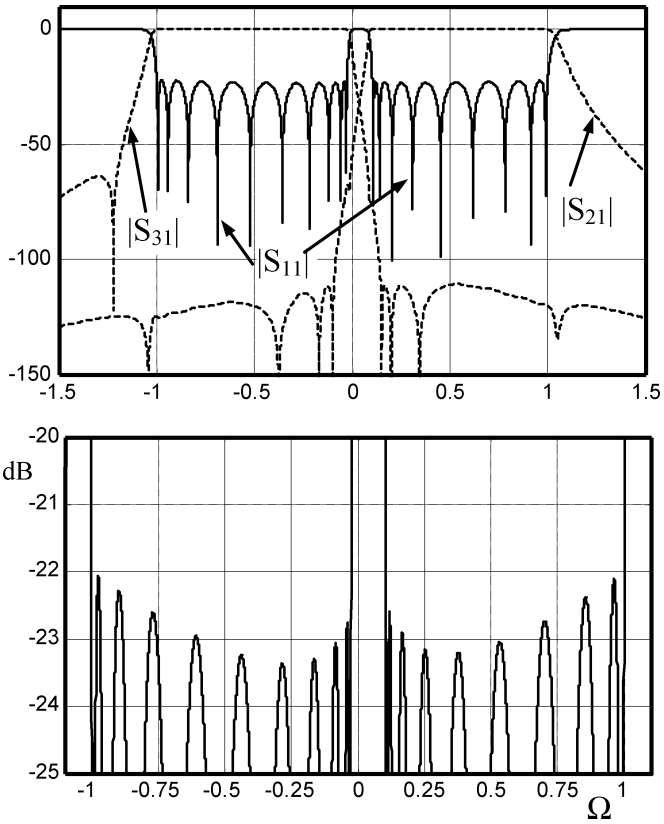

Fig. 9. Response of the diplexer with type-II junction evaluated through the characteristic polynomials (upper graph). The lower graph shows an expanded view of $|S_{11}|$ in the two passbands.

and $P^0_{\rm RX}$, $E^0_{\rm RX}$) are computed through the method described in [11], imposing the generalized Chebyshev characteristic with the required transmission zeros. The additional normalized reflection zero s_0 (imposed by the resonating junction) has been assigned to 1.5 (as suggested in Section IV). Fig. 9 shows the diplexer frequency response obtained from the computed polynomials. It also reports a close-up view of $|S_{11}|$ in the two passbands: it can be seen that the maximum peak-to-peak deviation of $|S_{11}|$ with respect to the equiripple condition is less that 1.5 dB. It is interesting to observe that, in addition to the imposed transmission zeros, the diplexer response exhibits additional transmission zeros (i.e., the zeros of $S_{\rm TX}$ and $S_{\rm RX}$), which contribute to the diplexer selectivity in the two filters stopband.

Continuing with the synthesis procedure, the normalized capacitance $c_0 = 0.398$ is obtained with (14) and the polynomials $P_{\rm TX}$, $F_{\rm TX}$, $E_{\rm TX}$, $P_{\rm RX}$, $F_{\rm RX}$, and $E_{\rm RX}$ are computed with (15)–(18). Two suitable low-pass prototypes have been then synthesized from such polynomials. The chosen topology of the prototypes is constituted by the cascade of triplets and/or quadruplets blocks, determining the required transmission zeros (the method described in [12] has been used for the synthesis).

Fig. 10 shows the resulting topology of the overall diplexer. Note that the required transmission zeros in the RX filter has been implemented through the cascade of four triplets, while the transmission zeros in the TX filter are obtained with a triplet cascaded with a quadruplet. The method described in [15] could also be employed for synthesizing the low-pass prototype of the overall diplexer (Fig. 10) in a single pass.

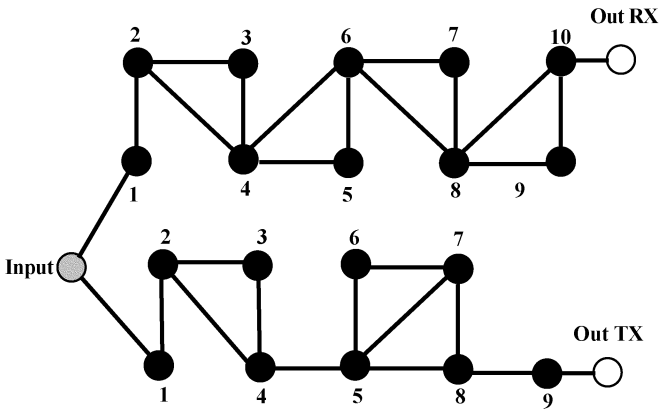

Fig. 10. Topology of the diplexer low-pass prototype. Each black node represents a unit capacitance in parallel with a frequency invariant susceptance $(M(k,k))$; the solid lines are admittance inverters $(M(i,j))$. The input node (gray) is the parallel of the capacitance c_0 with the unit source conductance; TX and RX loads (white nodes) are unit conductances.

Denormalization of the Diplexer Low-Pass Prototype

The diplexer low-pass prototype (Fig. 10) is globally characterized by means of the coupling matrices $M_{\rm TX}$ and $M_{\rm RX}$ obtained from the synthesis [12]. These matrices must be de-normalized for obtaining the parameters of filters and resonating junction to be used in the physical dimensioning of the diplexer (they are the coupling coefficients, resonating frequencies, and external Q's [16]). Using the properties of the coupling matrices and inverting the low-pass–bandpass transformation adopted here (Fig. 4), the following expressions are obtained (f_0 and B are defined in Fig. 4):

$$
\begin{aligned}
f_{ris} &= f_0 \text{ (resonant junction)} \\
B_n &= B/f_0 \\
f_0^{\rm RX}(k) &= f_0 \left[\sqrt{1 - \left(\frac{M_{\rm RX}(k,k) \cdot B_n}{2} \right)^2} \right. \\
&\qquad \left. - \left(\frac{M_{\rm RX}(k,k) \cdot B_n}{2} \right) \right] \\
f_0^{\rm TX}(k) &= f_0 \left[\sqrt{1 - \left(\frac{M_{\rm TX}(k,k) \cdot B_n}{2} \right)^2} \right. \\
&\qquad \left. - \left(\frac{M_{\rm TX}(k,k) \cdot B_n}{2} \right) \right] \\
k^{\rm TX}_{i,j} &= B_n M_{\rm TX}(i,j) \\
k^{\rm TX}_{0,1} &= \frac{B_n M_{\rm TX}(0,1)}{\sqrt{c_0}} \\
k^{\rm RX}_{i,j} &= B_n M_{\rm RX}(i,j) \\
k^{\rm RX}_{0,1} &= \frac{B_n M_{\rm RX}(0,1)}{\sqrt{c_0}} \\
Q_{\rm EXT,TX} &= \frac{1}{B_n M^2_{\rm TX}(np_{\rm TX}, np_{\rm TX}+1)} \\
Q_{\rm EXT,RX} &= \frac{1}{B_n M^2_{\rm RX}(np_{\rm RX}, np_{\rm RX}+1)} \\
Q_{\rm EXT} &= \frac{c_0}{B_n}.
\end{aligned}
\tag{21}
$$

Note that $k_{0,1}^{\mathrm{TX}}$ and $k_{0,1}^{\mathrm{RX}}$ represent the coupling coefficients between the input resonating node and the first TX and RX resonators, respectively. Q_{EXT} represents the external Q of the resonating junction loaded by the source conductance. $Q_{\mathrm{EXT,TX}}$ and $Q_{\mathrm{EXT,RX}}$ are the external Q's determined by the loads at ports 2 and 3 of the diplexer on the last resonators in the TX and RX filters.

The following values have been obtained for the synthesized diplexer.

- TX filter:
  Main path coupling coefficients $(k_{12} \ldots k_{89})$: [0.0239, 0.0177, 0.0168, 0.0185, 0.0148, 0.0138, 0.0204, 0.0295].
  Cross-coupling coefficients: $k_{24} = -0.0086$; $k_{58} = 0.0022$; $k_{57} = -0.0111$; $Q_{\mathrm{EXT,TX}} = 26.97$.
  f_0^{TX} (MHz): [1963.77 1960.46 1943.24 1959.64 1959.5 1937.67 1956.38 1958.6 1958.43].
- RX filters:
  Main path coupling coefficients $(k_{12} \ldots k_{910})$: [0.0257, 0.0190, 0.0177, 0.0187, 0.0186, 0.0176, 0.0181, 0.0183, 0.0280].
  Cross-coupling coefficients: $k_{24} = -0.0095$; $k_{46} = 0.0066$; $k_{68} = 0.0095$; $k_{810} = 0.0151$; $Q_{\mathrm{EXT,RX}} = 24.9$.
  f_0^{RX} (MHz): [1875.02 1878.18 1862.8 1880.24 1892.07 1879.21 1896.56 1877.32 1899.54 1880.23].
- Resonating junction parameters:
  f_0 (MHz): 1917.36.
  External Q_{EXT}: 5.21.
  First TX coupling: $k_{0,1}^{\mathrm{TX}} = 0.071252$.
  First RX coupling: $k_{0,1}^{\mathrm{RX}} = 0.073636$.

From the above parameters, the physical dimensioning of the diplexer can be performed, employing well-known methods available in the literature [16], [17].

Fabrication and Testing

For validating the novel method, the designed diplexer has been fabricated employing comb coaxial cavities coupled through apertures in the common walls and tuned with screws at the inner conductor open end. Nonadjacent couplings have been realized with suitable capacitive or inductive probes. The required external Q's are obtained through taps on the inner rod of the last resonators in each filter ($Q_{\mathrm{EXT,TX}}$ and $Q_{\mathrm{EXT,RX}}$) and on the rod constituting the resonating junction (Q_{EXT}).

A schematic draw of the realized diplexer is shown in Fig. 11. The length of the cavities in each filter is approximately $\lambda_0/8$ (where the wavelength λ_0 is evaluated at the center of each filter passband). The diplexer cover (not shown in this figure) includes the tuning screws employed for alignment purposes.

Fig. 12 reports the measured attenuation and return loss of the diplexer with the best realized alignment in the two passbands. For comparison, the simulated response of the diplexer (obtained from the diplexer polynomials) is also reported in this figure.

It can be observed that the agreement between the measured and simulated curves is very satisfactory (measurement accuracy is scarcely above -80 dB for the relatively high noise floor

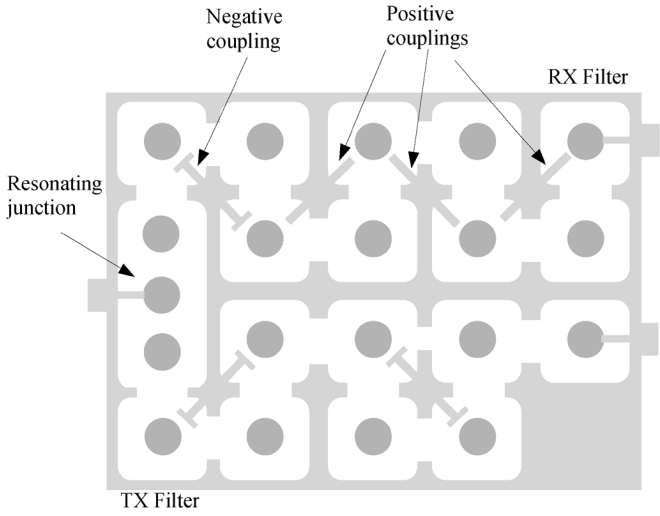

Fig. 11. Top view of the fabricated diplexer.

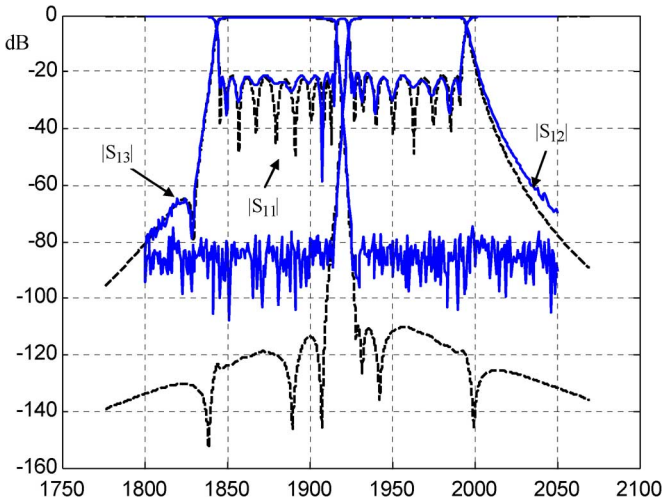

Fig. 12. Measured (solid line) and simulated (dashed line) diplexer response. From [9]. (Color version available online at http://ieeexplore.ieee.org.)

of the scalar network analyzer employed; however, the agreement in the two passbands is well evident).

VII. Conclusion

An innovative approach to the synthesis of microwave diplexers has been presented. The main feature of this approach is the evaluation through an iterative procedure of the characteristic polynomials associated to a specific diplexer topology (two types of three-port junctions connecting the RX and TX filters have been considered). The characteristic polynomials of the filters are then evaluated from the diplexer polynomials, and their synthesis is performed separately from the diplexer (the filters topology is arbitrary with allowed complex transmission zeros). The synthesized filters take into account the mutual loading effect produced by their connection to the three-port junction. The simulation of the synthesized diplexer (described with a network model) gives a quasi-equiripple response in the TX and RX frequency bands (the response deviates less than 2 dB from the perfect equiripple characteristic in all cases

considered). The novel synthesis approach gives the best performance with very close diplexer channels (even contiguous). The design accuracy may be poor, on the other hand, with widely spaced channels because the polynomial models of microwave filters become more and more inaccurate as the normalized bandwidth increases (in fact, the normalized bandwidth employed in the bandpass—low-pass transformation depends on the difference between the outer limits of the TX and RX bands).

By applying specific de-normalizing formulas (presented in this paper for the considered diplexer topologies), suitable parameters can be evaluated allowing a first-order dimensioning of the diplexer. The design results can be then employed either for the fabrication of the diplexer (if tuning elements are allowed in the structure) or as a starting point for a full-wave optimization of the overall structure when very high accuracy is required (as in case of no tuning elements employed).

Two implementations of the synthesis procedure have been reported, concerning waveguide and coaxial diplexers. The validation of the procedure in case of diplexers employing tuning elements has been obtained through the fabrication of the coaxial diplexer (a device for GSM 1900-MHz base stations): the measured response of the fabricated device (after the best alignment) is in excellent agreement with the expected response computed through the polynomial model of the diplexer.

The extension of the presented synthesis technique to triplexers and multiplexers may be possible in case of lumped junctions (structures based on manifold are then excluded).

REFERENCES

[1] J. D. Rhodes, "Direct design of symmetrical interacting bandpass channel diplexer," *Inst. Elect. Eng. J.—Microw., Opt., Acoust.*, vol. I, no. 1, pp. 34–40, Sep. 1976.

[2] J. L. Haine and J. D. Rhodes, "Direct design formulas for asymmetric bandpass channel diplexers," *IEEE Trans. Microw. Theory Tech.*, vol. MTT-25, no. 10, pp. 807–813, Oct. 1977.

[3] R. Levy, "Synthesis of non-contiguous diplexers using broadband matching theory," in *IEEE MTT-S Int. Microw. Symp. Dig.*, 1991, pp. 543–545.

[4] M. Guglielmi, "Optimum CAD procedure for manifold diplexers," in *IEEE MTT-S Int. Microw. Symp. Dig.*, 1993, pp. 1081–1084.

[5] Y. Rong, H.-W. Yao, K. A. Zaki, and T. G. Dolan, "Millimeter-wave $K\alpha$-band H-plane diplexers and multiplexers," *IEEE Trans. Microw. Theory Tech.*, vol. 47, no. 12, pp. 2325–2330, Dec. 1999.

[6] A. Morini and T. Rozzi, "Constraints to the optimum performance and bandwidth limitations of diplexers employing symmetric three-port junctions," *IEEE Trans. Microw. Theory Tech.*, vol. 40, no. 2, pp. 242–248, Feb. 1996.

[7] L. Accattino and M. Mongiardo, "Hybrid circuit-full-wave computer-aided design of a manifold multiplexers without tuning elements," *IEEE Trans. Microw. Theory Tech.*, vol. 50, no. 9, pp. 2044–2047, Sep. 2002.

[8] R. J. Cameron, "Advanced coupling matrix synthesis techniques for microwave filters," *IEEE Trans. Microw. Theory Tech.*, vol. 51, pp. 1–10, Jan. 2003.

[9] G. Macchiarella and S. Tamiazzo, "Synthesis of diplexers based on the evaluation of suitable characteristic polynomials," in *IEEE MTT-S Int. Microw. Symp. Dig.*, 2006, pp. 111–114.

[10] N. Marcuvitz, *Waveguide Handbook*. NewYork: Dover, 1965.

[11] G. Macchiarella, "Accurate synthesis of in-line prototype filters using cascaded triplet and quadruplet sections," *IEEE Trans. Microw. Theory Tech.*, vol. 50, no. 7, pp. 1779–1783, Jul. 2002.

[12] S. Tamiazzo and G. Macchiarella, "An analytical technique for the synthesis of cascaded N-tuplets cross-coupled resonators microwave filters using matrix rotations," *IEEE Trans. Microw. Theory Tech.*, vol. 53, no. 5, pp. 1693–1698, May 2005.

[13] G. L. Matthaei, L. Young, and E. M. T. Jones, *Microwave Filters, Impedance-Matching Networks and Coupling Structures*. Norwood, MA: Artech House, 1980, ch. 8.

[14] R. Levy, "Theory of direct-coupled-cavity filters," *IEEE Trans. Microw. Theory Tech.*, vol. MTT-15, no. 6, pp. 340–348, Jun. 1967.

[15] A. Garcia-Lampérez, M. Salazar-Palma, and T. K. Sarkar, "Analytical synthesis of microwave multiport networks," in *IEEE MTT-S Int. Microw. Symp. Dig.*, 2004, pp. 455–458.

[16] H.-W. Yao, J.-F. Liang, and K. A. Zaki, "Accuracy of coupling computations and its application to DR filter design," in *IEEE MTT-S Int. Microw. Symp. Dig.*, 1994, pp. 723–726.

[17] G. Macchiarella, "An original approach to the design of bandpass cavity filters with multiple couplings," *IEEE Trans. Microw. Theory Tech.*, vol. 45, no. 2, pp. 179–187, Feb. 1997.

Giuseppe Macchiarella (M'88) was born in Milan, Italy, in 1952. He received the Laurea degree in electronic engineering from the Politecnico di Milano, Milan, Italy, in 1975.

From 1977 to 1987, he was a Researcher with the National Research Council of Italy, where he was involved in studies on microwave propagation. In 1987, he became Associate Professor of microwave engineering with the Dipartimento di Elettronica e Informazione, Politecnico di Milano. His current research is in the field of microwave circuits with special emphasis on microwave filters synthesis and power amplifier linearization. He has authored or coauthored over 80 papers and conference presentations.

Stefano Tamiazzo received the Laurea degree in telecommunication engineering from the Politecnico di Milano, Milan, Italy, in 2002, and the Master degree in Information Technology from Cefriel, Milan, Italy, in 2003.

He is currently with Andrew Telecommunication Products, Agrate Brianza, Italy, where he is involved in the design of microwave filters and combiners for wireless applications.

射 频 和 天 线 设 计 培 训 课 程 推 荐

易迪拓培训(www.edatop.com)由数名来自于研发第一线的资深工程师发起成立，致力并专注于微波、射频、天线设计研发人才的培养；我们于 2006 年整合合并微波 EDA 网(www.mweda.com)，现已发展成为国内最大的微波射频和天线设计人才培养基地，成功推出多套微波射频以及天线设计经典培训课程和 ADS、HFSS 等专业软件使用培训课程，广受客户好评；并先后与人民邮电出版社、电子工业出版社合作出版了多本专业图书，帮助数万名工程师提升了专业技术能力。客户遍布中兴通讯、研通高频、埃威航电、国人通信等多家国内知名公司，以及台湾工业技术研究院、永业科技、全一电子等多家台湾地区企业。

易迪拓培训课程列表：http://www.edatop.com/peixun/rfe/129.html

射频工程师养成培训课程套装

该套装精选了射频专业基础培训课程、射频仿真设计培训课程和射频电路测量培训课程三个类别共 30 门视频培训课程和 3 本图书教材；旨在引领学员全面学习一个射频工程师需要熟悉、理解和掌握的专业知识和研发设计能力。通过套装的学习，能够让学员完全达到和胜任一个合格的射频工程师的要求…

课程网址：http://www.edatop.com/peixun/rfe/110.html

ADS 学习培训课程套装

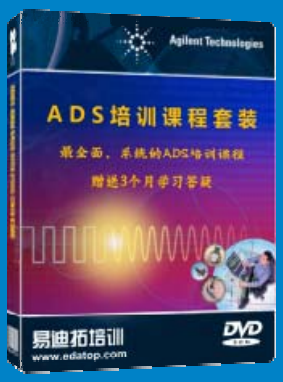

该套装是迄今国内最全面、最权威的 ADS 培训教程，共包含 10 门 ADS 学习培训课程。课程是由具有多年 ADS 使用经验的微波射频与通信系统设计领域资深专家讲解，并多结合设计实例，由浅入深、详细而又全面地讲解了 ADS 在微波射频电路设计、通信系统设计和电磁仿真设计方面的内容。能让您在最短的时间内学会使用 ADS，迅速提升个人技术能力，把 ADS 真正应用到实际研发工作中去，成为 ADS 设计专家...

课程网址： http://www.edatop.com/peixun/ads/13.html

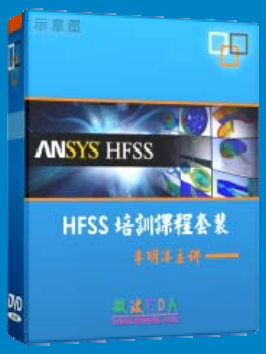

HFSS 学习培训课程套装

该套课程套装包含了本站全部 HFSS 培训课程，是迄今国内最全面、最专业的 HFSS 培训教程套装，可以帮助您从零开始，全面深入学习 HFSS 的各项功能和在多个方面的工程应用。购买套装，更可超值赠送 3 个月免费学习答疑，随时解答您学习过程中遇到的棘手问题，让您的 HFSS 学习更加轻松顺畅…

课程网址：http://www.edatop.com/peixun/hfss/11.html

CST 学习培训课程套装

该培训套装由易迪拓培训联合微波 EDA 网共同推出，是最全面、系统、专业的 CST 微波工作室培训课程套装，所有课程都由经验丰富的专家授课，视频教学，可以帮助您从零开始，全面系统地学习 CST 微波工作的各项功能及其在微波射频、天线设计等领域的设计应用。且购买该套装，还可超值赠送 3 个月免费学习答疑…

课程网址：http://www.edatop.com/peixun/cst/24.html

HFSS 天线设计培训课程套装

套装包含 6 门视频课程和 1 本图书，课程从基础讲起，内容由浅入深，理论介绍和实际操作讲解相结合，全面系统的讲解了 HFSS 天线设计的全过程。是国内最全面、最专业的 HFSS 天线设计课程，可以帮助您快速学习掌握如何使用 HFSS 设计天线，让天线设计不再难…

课程网址：http://www.edatop.com/peixun/hfss/122.html

13.56MHz NFC/RFID 线圈天线设计培训课程套装

套装包含 4 门视频培训课程，培训将 13.56MHz 线圈天线设计原理和仿真设计实践相结合，全面系统地讲解了 13.56MHz 线圈天线的工作原理、设计方法、设计考量以及使用 HFSS 和 CST 仿真分析线圈天线的具体操作，同时还介绍了 13.56MHz 线圈天线匹配电路的设计和调试。通过该套课程的学习，可以帮助您快速学习掌握 13.56MHz 线圈天线及其匹配电路的原理、设计和调试…

详情浏览：http://www.edatop.com/peixun/antenna/116.html

我们的课程优势：

※ 成立于 2004 年，10 多年丰富的行业经验，

※ 一直致力并专注于微波射频和天线设计工程师的培养，更了解该行业对人才的要求

※ 经验丰富的一线资深工程师讲授，结合实际工程案例，直观、实用、易学

联系我们：

※ 易迪拓培训官网：http://www.edatop.com

※ 微波 EDA 网：http://www.mweda.com

※ 官方淘宝店：http://shop36920890.taobao.com